The Fifth International Bridge Seismic Workshop (5IBSW)
Hunan University, Changsha, China, June 5-7, 2026

Effective Vibration Length Identification and Cable Force Estimation of Stay Cables Based on UAV Video: Integrating Multi-Order Mode-Shape Consistency Constraints and SSD-CEEMDAN Drift Separation

Supervisor ： Prof. Pengzhen Lin　　Presenter: Yahui Qi

1.1 Research background

Direct measurement / Strain-based method / Vibration-frequency method / Vision-based method

pressure sensors, etc.

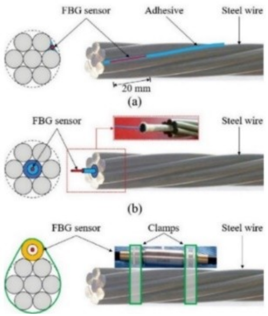

fiber Bragg grating sensors, etc.

accelerometer

fixed cameras and UAVs

UAV-based vibration measurement

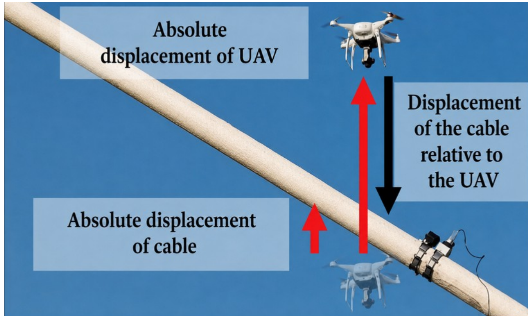

- Feature tracking
- Optical flow method
- Deep-learning

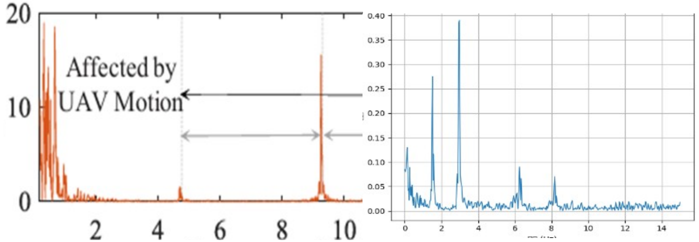

UAV platform drift

1.2 Research background

Mode Shape Identification Using Acceleration

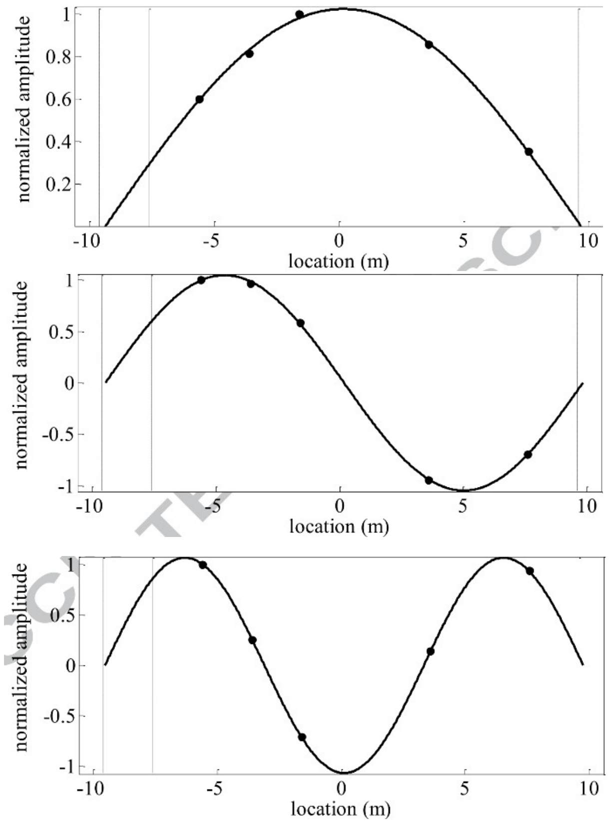

Chien-Chou Chen, Wen-Hwa Wu, Min-Ray Leu, and Gwolong Lai. Tension determination of stay cable or external tendon with complicated constraints using multiple vibration measurements. Measurement, 86:182–195, 2016.

1.1 Research Background

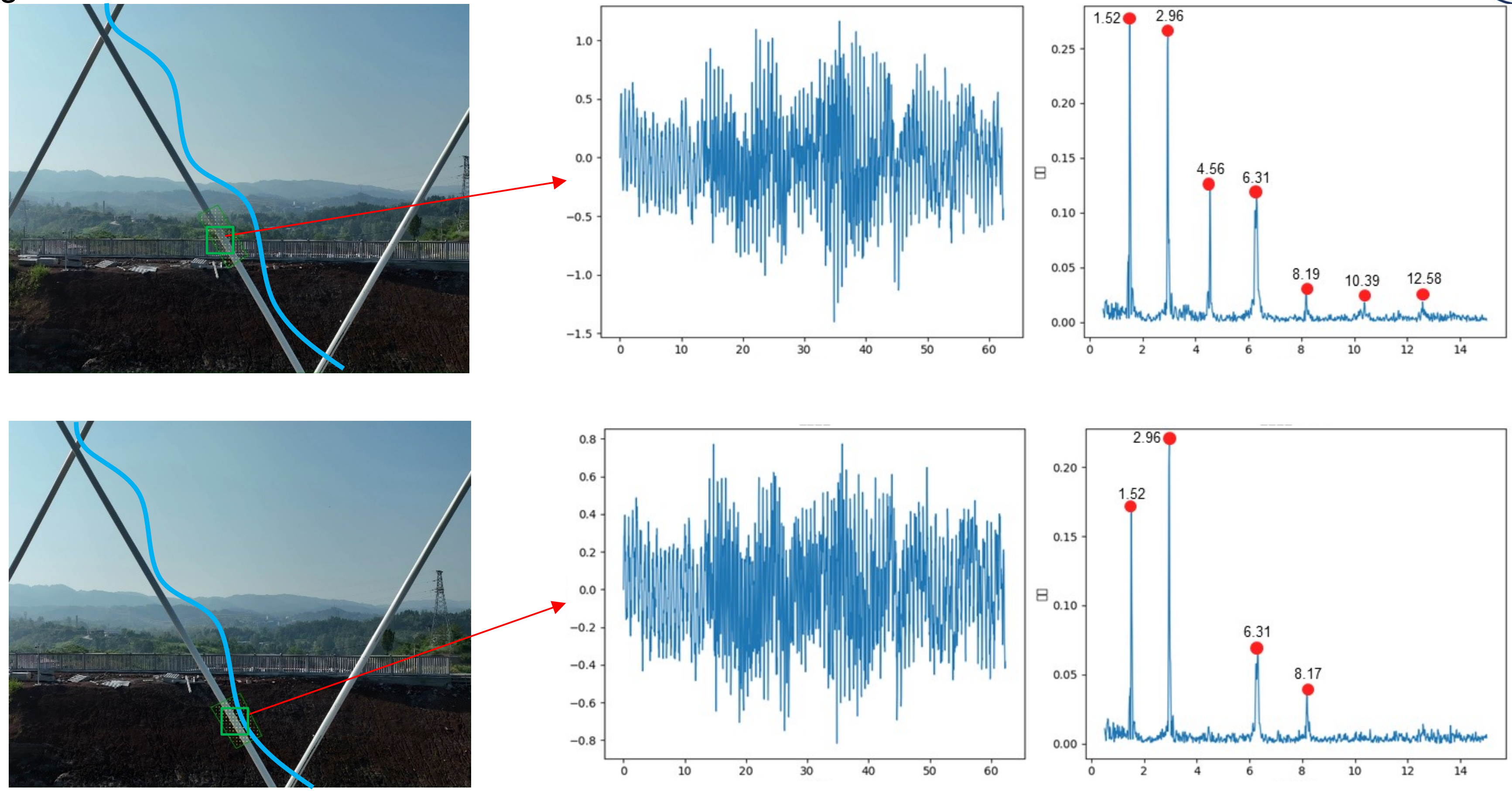

2.1 Pipeline overview

Current Existing Problems

- Non-ideal pinned boundary conditions
- Difficulty in measuring cable length
- Difficulty in installing acceleration sensors

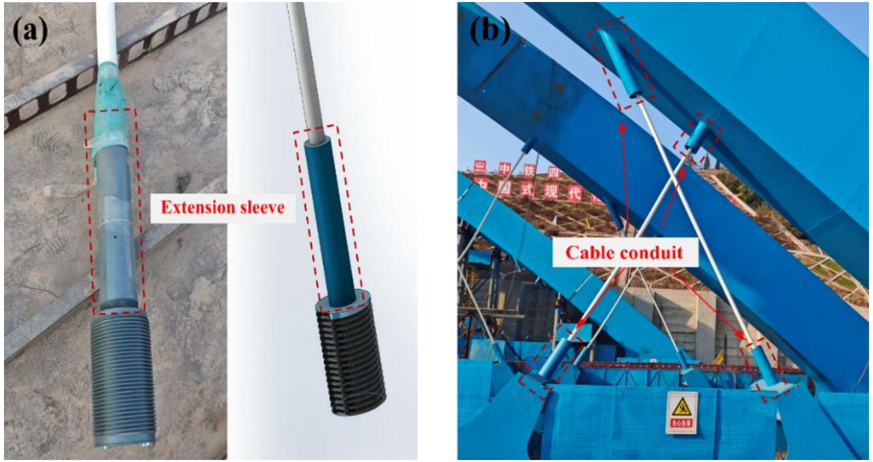

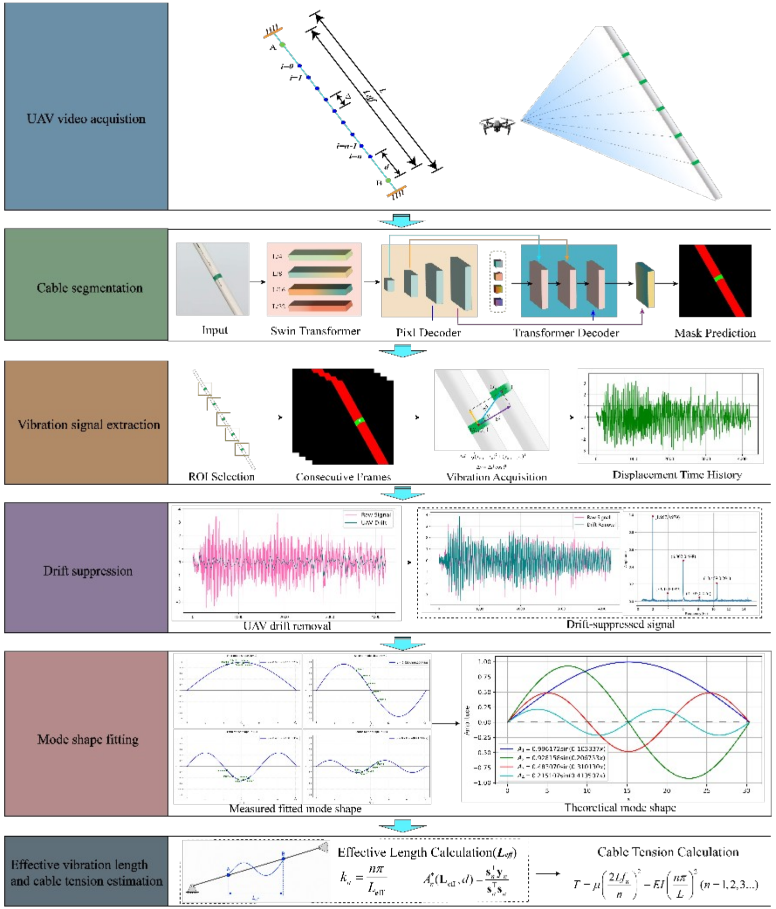

2.2 UAV-based vibration displacement extraction

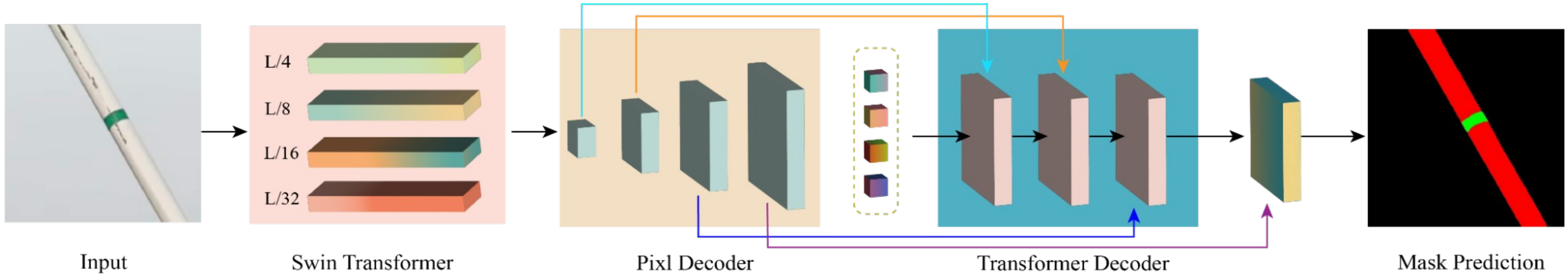

Mask2former

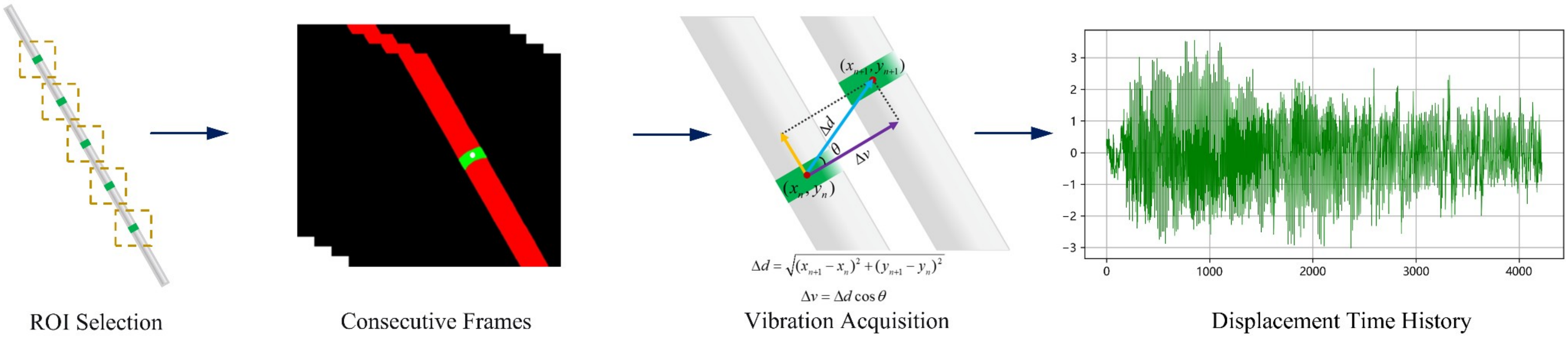

Vibration extraction flowchart

2.3 Effect of UAV Drift on Cable Vibration Measurement

2.3 UAV drift suppression

Only the background is moving

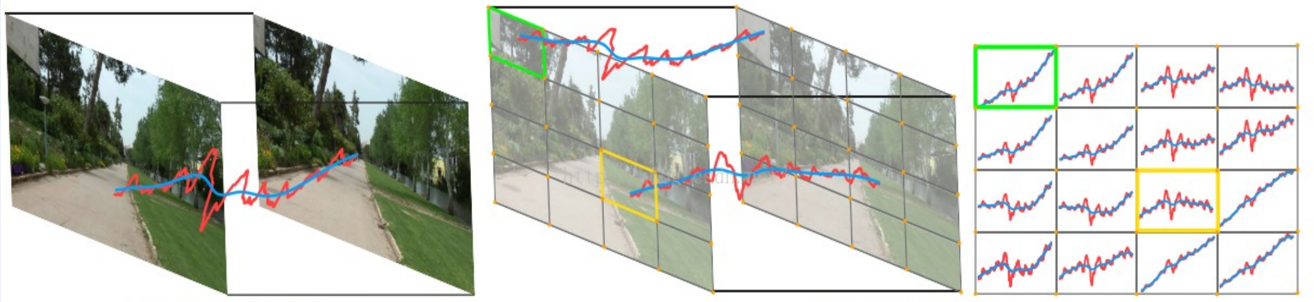

(a) a single global path (b) our bundled paths

Global image motion caused by camera shake

Background and the cable are moving

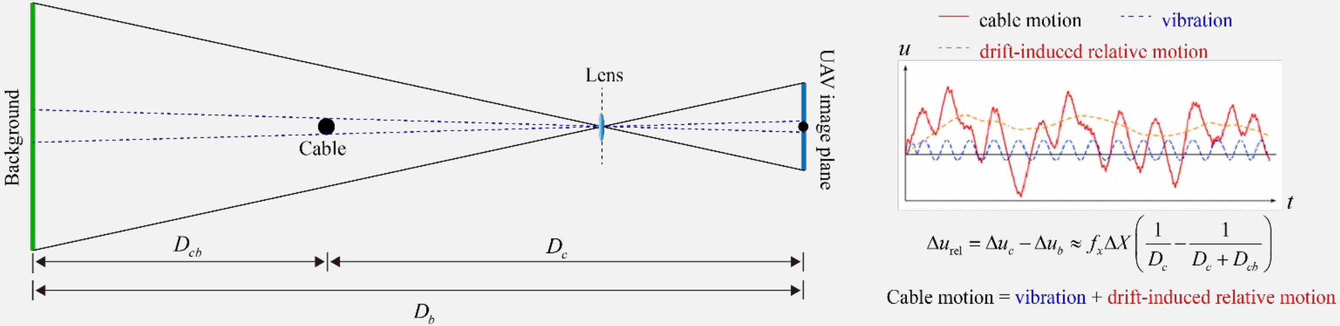

Both the background and the cable are moving

https://github.com/Nicolas91B/imageStabilization/blob/master/imageStabilization.cpp

Cai, Enjian, Yi Zhang, Xinzheng Lu, Peipei Li, Taisen Zhao, Guangwei Lin, and Wei Guo. "A target-free video structural motion estimation method based on multi-path optimization." Mechanical Systems and Signal Processing 198 (2023): 110452.

2.3 UAV drift suppression

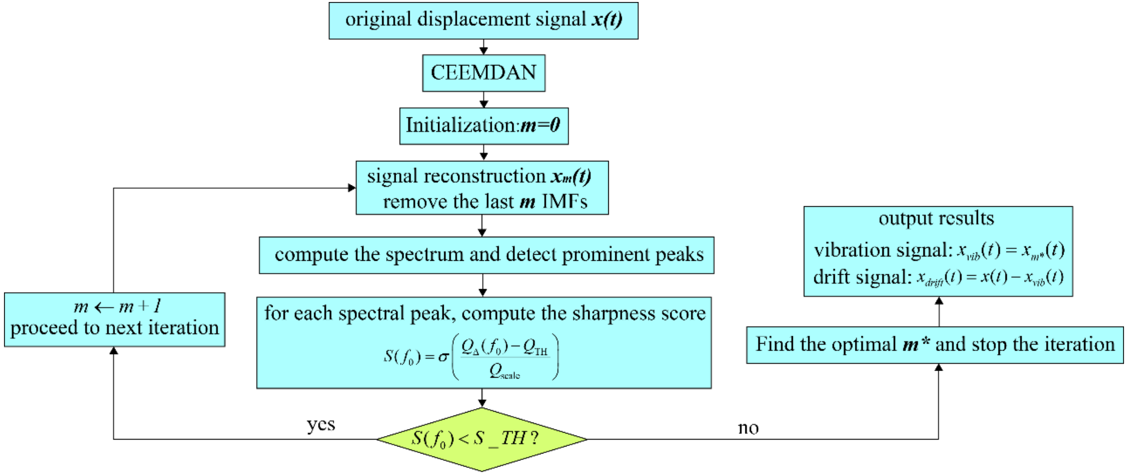

SSD-CEEMDAN drift separation flowchart

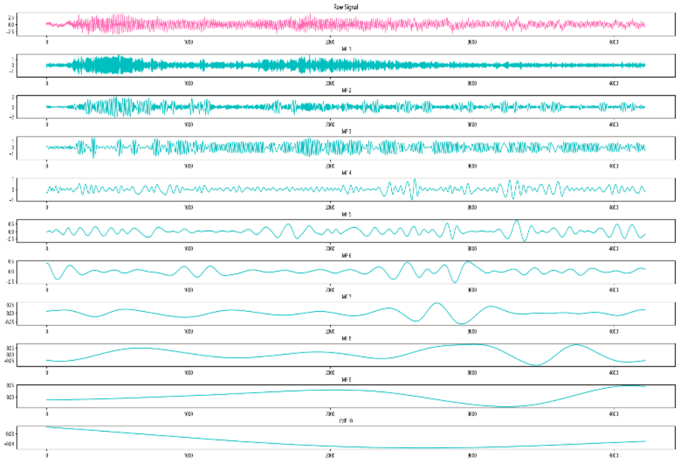

CEEMDAN decomposition

CEEMDAN yields K IMFs and residual r(t)：

$$x(t)=\sum_{i=1}^{K} IMF_i(t)+r(t)$$

The low-frequency components removed accordingly are:

$$x_m(t)=x(t)-\sum_{i=K-m+1}^{K} IMF_i(t)$$

Sharpness Score：

$$S(f_0)=\sigma\left(\frac{Q_\Delta(f_0)-Q_{TH}}{Q_{scale}}\right),\quad \sigma(x)=\frac{1}{1+e^{-x}}$$

The stopping criterion is: $S(f_0)\geq S_{TH}$

True vibration is defined as:

$$x_{vib}(t)=x_{m^*}(t)=\sum_{i=1}^{K-m^*} IMF_i(t)$$

Drift component:

$$x_{drift}(t)=x(t)-x_{vib}(t)=\sum_{i=K-m^*+1}^{K} IMF_i(t)$$

2.4 Effective vibration length identification

Observation model：

$$y_{i} = A_{n}\sin\left(\frac{n\pi}{L_{\mathrm{eff}}}x_{i}\right)$$

Joint least-squares objective function：

$$\min_{L_{\mathrm{eff}},d}\sum_{n=1}^{N}\sum_{i=1}\left[y_{n,i}-A_{n}\sin\left(\frac{n\pi}{L_{\mathrm{eff}}}(x_{i}+d)\right)\right]^{2}$$

Two-layer variable elimination strategy：

$$\sin\left(\frac{n\pi}{L_{\mathrm{eff}}}(x_{i}+d)\right)$$

Closed-form least-squares solution:

$$A_{n}^{*}(L_{\mathrm{eff}},d)=\frac{s_{n}^{T}y_{n}}{s_{n}^{T}s_{n}}$$

After obtaining the optimal L^{*}_{eff} and d^{*}, the node positions of the n-th mode shape can be expressed as:

$$x_{k}=\frac{k}{n}L^{*}_{\mathrm{eff}}-d^{*}$$

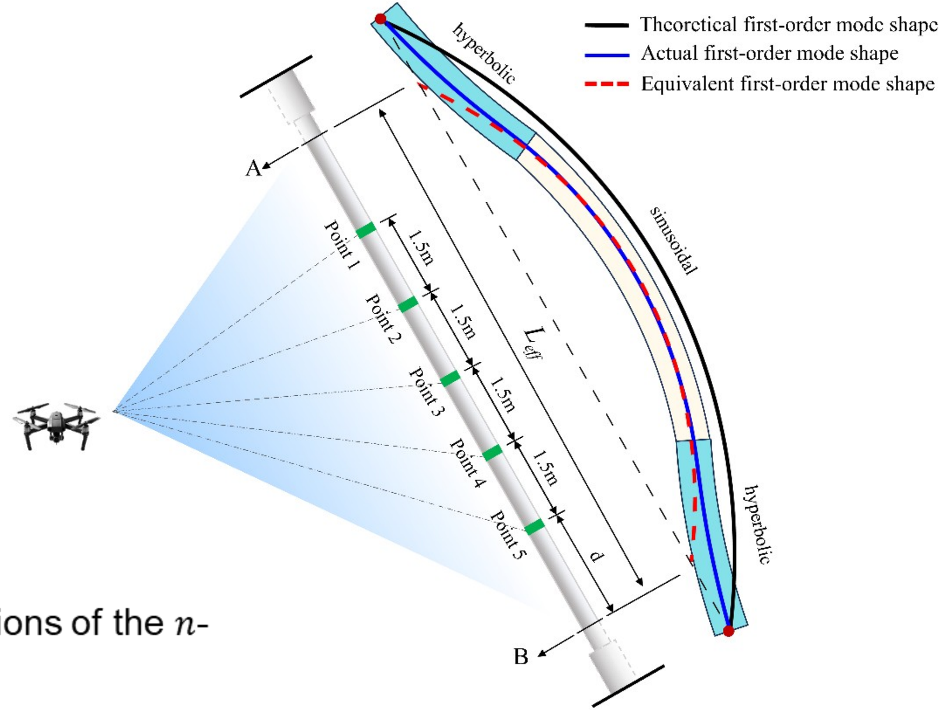

Actual cable mode-shape function:

$$\varphi_{k}(x)=\varphi_{k}^{(s)}(x)+\varphi_{k}^{(h)}(x)=\sin(\delta_{k}x)\pm\sin(\delta_{k}(1-x))-\frac{\sin(\delta_{k}x)}{\sinh(\gamma_{k})}\left[\sinh(\gamma_{k}x)\pm\sinh(\gamma_{k}(1-x))\right]$$

2.4 Measurement point layout

The cable mode shape can be approximately expressed in the form of a simple harmonic function:

[illegible]

At least three independent measurement points are theoretically required.

The spatial half-wavelength of the n-th mode is given by:

$$\frac{\lambda_n}{2} = \frac{L_{eff}}{n}$$

To avoid insufficient spatial sampling:

$$\Delta < \frac{L_{eff}}{n_{max}}$$

To stably capture mode-shape variation within a half-wavelength, the spacing can be further specified as:

$$\Delta \leq \frac{L_{eff}}{3n_{max}}$$

The measurement-point spacing should not be too small; otherwise, the local sinusoidal curve may become nearly linear, increasing fitting errors. Ideally, the measurement points should cover the node-to-antinode region, or at least a segment with evident curvature variation.

2.5 Effective bending stiffness calculation

The effective bending stiffness of stay cables is jointly affected by **end constraints, pretension, and inter-wire slip.**

Effective bending stiffness ≈ 40% of full-section bending stiffness [1-2]

The full-section bending stiffness of the stay cable can be expressed as:

$$EI_{full} = \text{[illegible]}$$

The hexagonal close-packed arrangement of the stay cable is:

$$1+6+12+18+24+30=91$$

When the wire bundle works fully compositely:

$$I_{full} = \text{[illegible]} \qquad EI_{full} = \text{[illegible]}$$

Using a 40% reduction coefficient, the effective bending stiffness of the stay cable is:

$$EI_{eff} = \text{[illegible]}$$

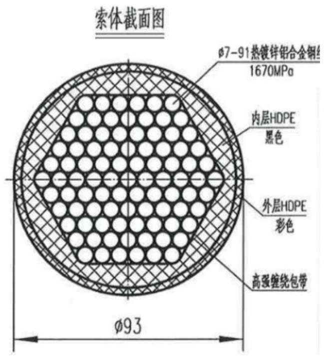

[1] Guo L. L., Liu H. B., Chen Z. H. Experimental research on the bending performance of locked coil wire rope and Galfan strand. Construction and Building Materials, 2021, 304: 124667.

[2] Shimada T. Estimating Method of Cable Tension From Natural Frequency of High Mode[J]. Doboku Gakkai

3.1 Project overview

The bridge has a total length of approximately 147 m, a deck width of approximately 17 m, and a total structural weight of about 2600 t. A total of 84 stay cables are installed, each with an outer diameter of approximately 9 cm. The cables are made of high-strength hot-dip galvanized aluminum alloy steel wires, with a tensile strength of 1670 MPa and an elastic modulus of 1.90×10^5 MPa. Each cable consists of 91 steel wires with a diameter of 7 mm, wrapped with a hot-extruded HDPE sheath.

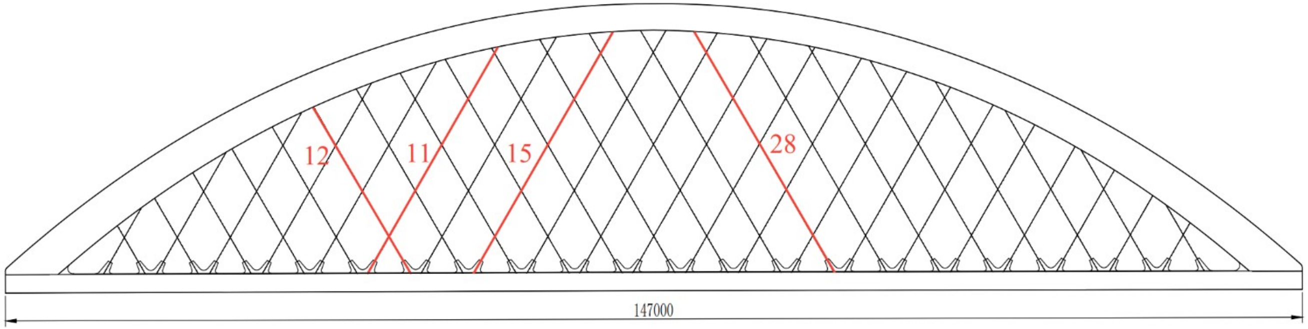

Under-construction experimental bridge.

3.2 Stay cable segmentation

Stay Cable Segmentation Based on Mask2Former

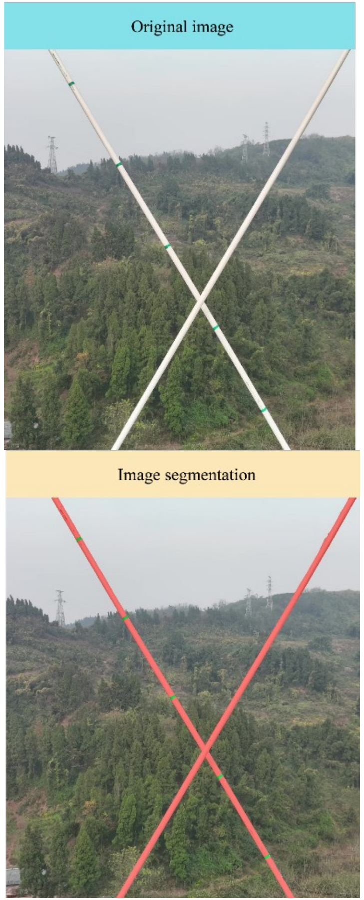

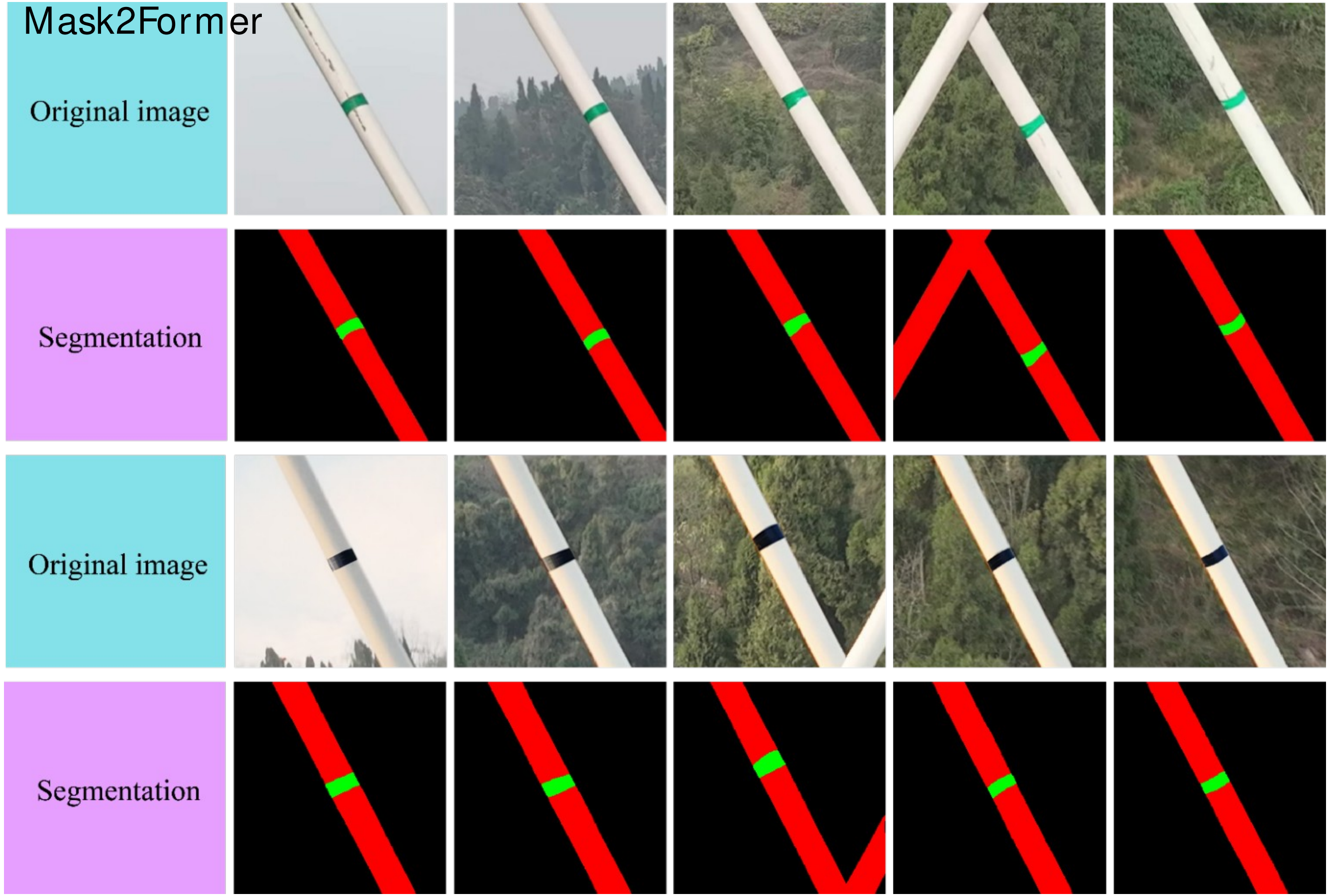

3.2 Vibration extraction

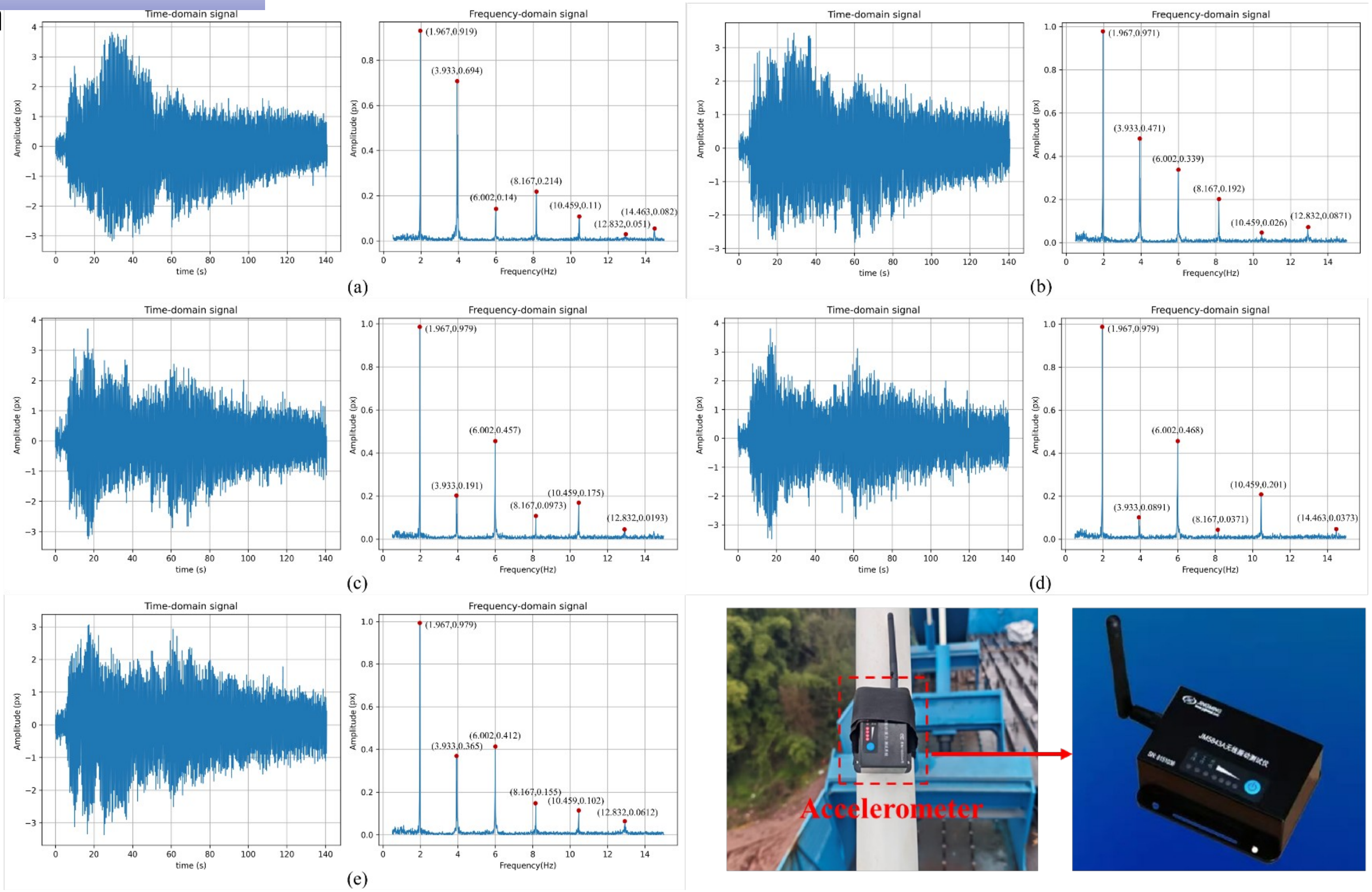

Measurement point vibration signal.(a)Point 1; (b)Point 2; (c)Point 3; (d)Point 4; (e)Point 5; (f)Accelerometer

Optical flow method, accelerometer, and proposed method comparison

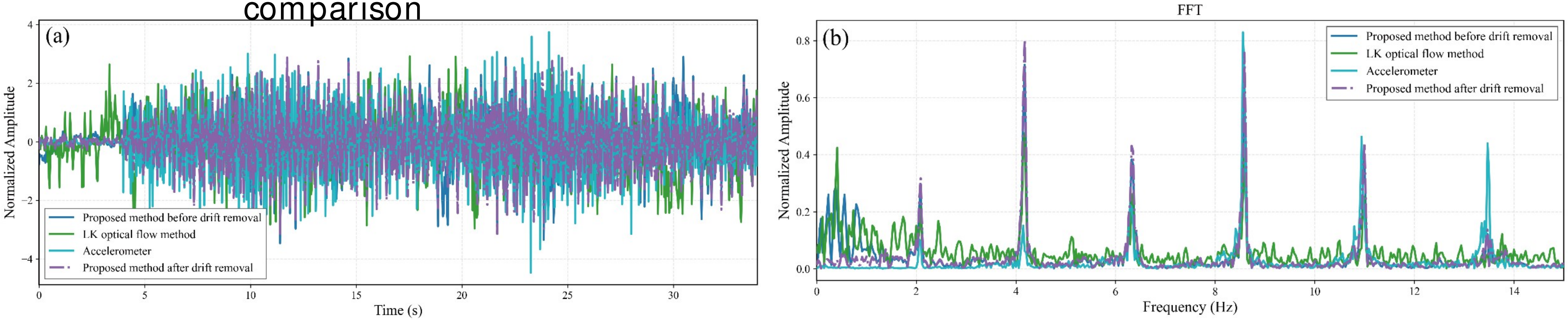

Vibration testing comparison. (a) Time-domain; (b) Frequency-domain

Table 1 Comparison of identified modal frequencies by different methods

Order	LK	Accelerometer	Proposed method (before drift removal)	Proposed method (after drift removal)
1	2.084	2.072	2.081	2.081
2	4.153	4.145	4.153	4.153
3	6.320	6.308	6.316	6.316
4	8.586	8.566	8.582	8.584
5	10.992	10.951	10.992	10.992
6	13.761	13.474	13.467	13.467

3.3 UAV drift suppression

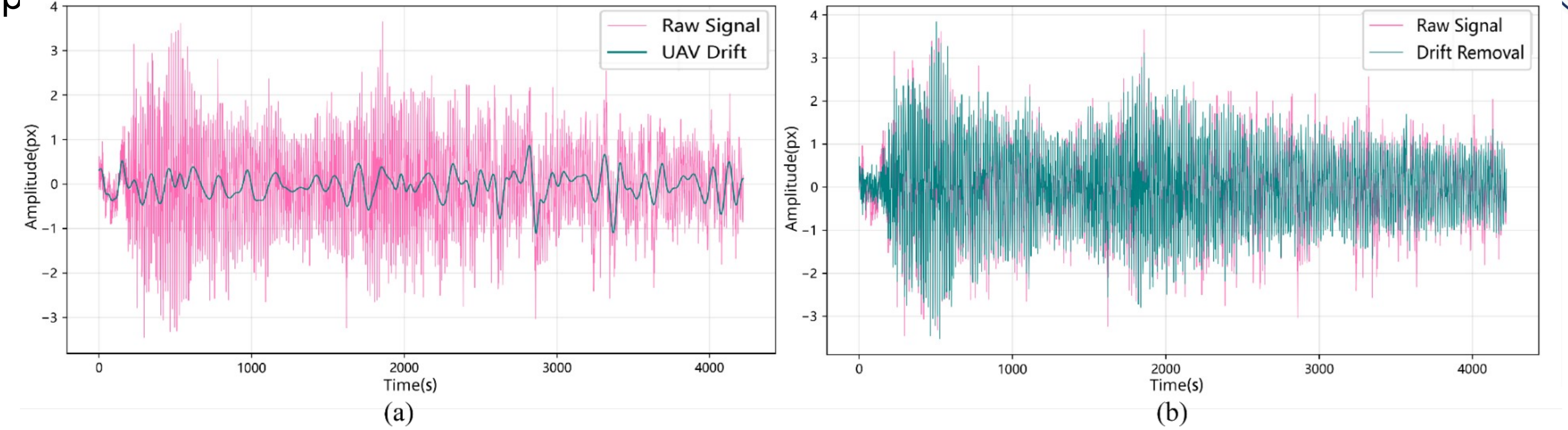

UAV drift signal separation. (a) UAV drift signal; (b) cable vibration signal after drift removal.

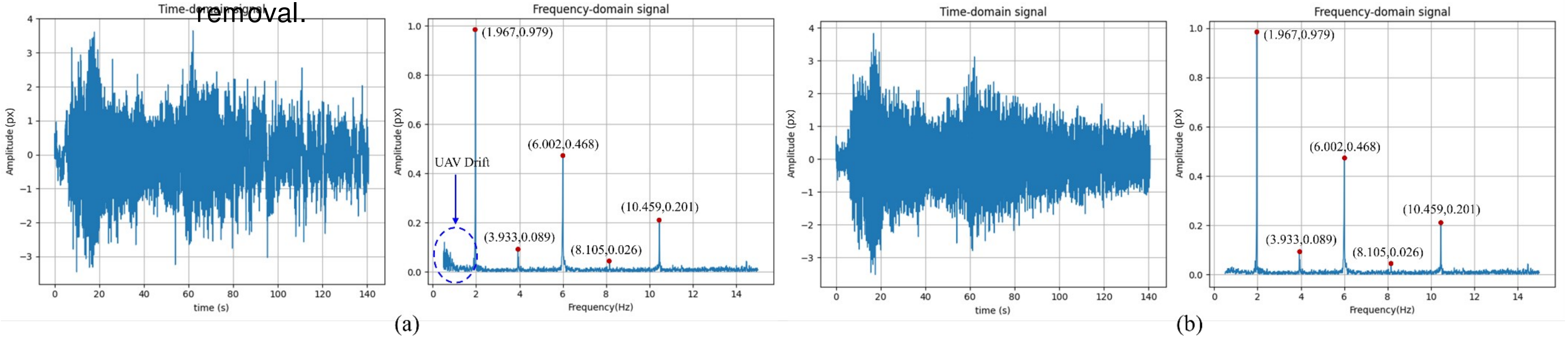

Drift signal removal. (a) Original signal; (b) signal after drift removal.

3.4 Mode shape fitting

d= 11.110626 m

x= {11.110626, 12.610626, 14.112626, 15.610626, 17.110626}m

$A_1 = 0.996172 sin 0.103337 x$

[illegible]

[illegible]

[illegible]

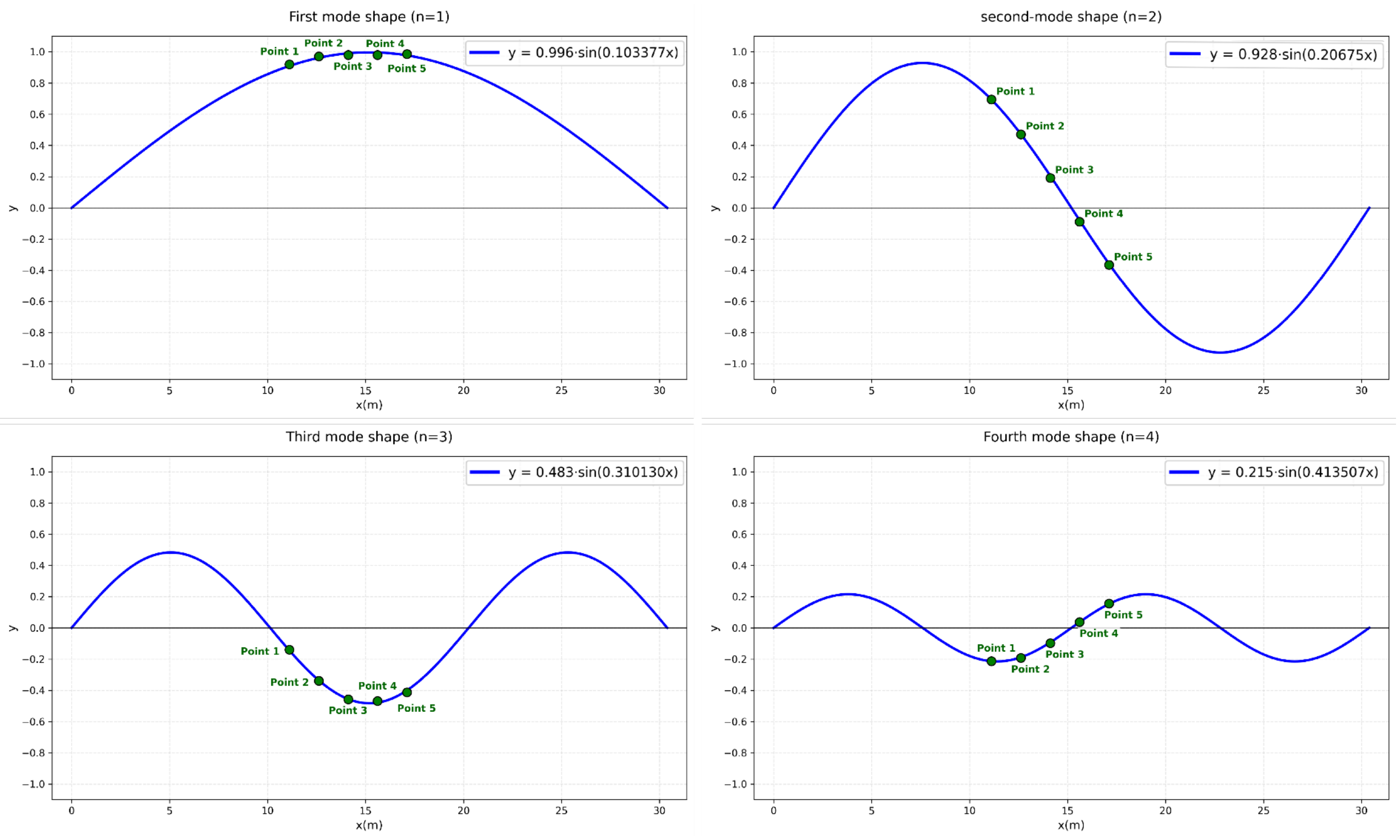

1st to 4th order modal shape fitting results

3.4 Finite element mode shapes

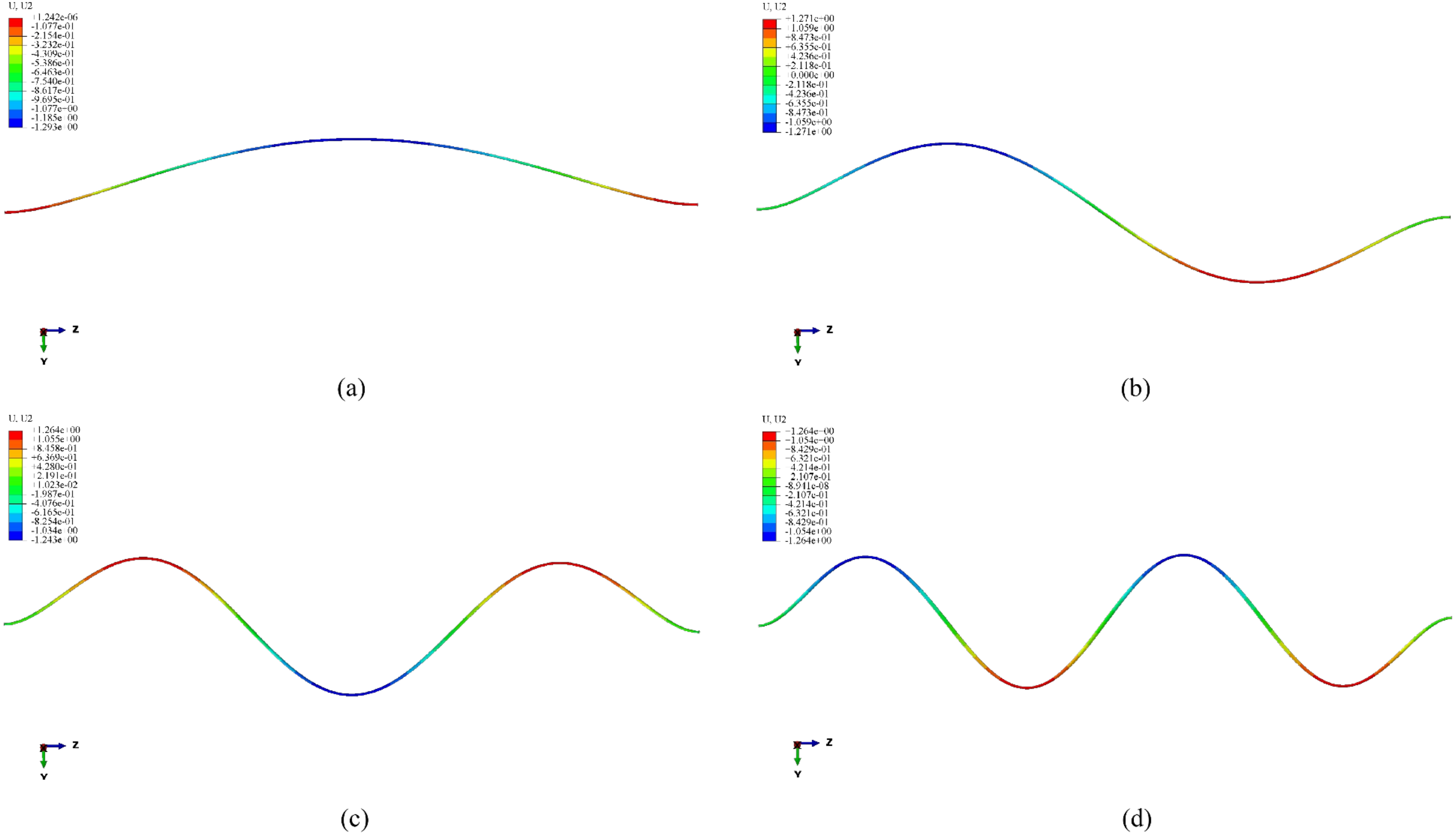

Finite element simulation of the First four modal shapes

3.4 Cable No. 15 fitting analysis

Table 3 Normalized amplitudes for different modes at each measurement point.

Mode	1st	2nd	3rd	4th
Measurement Point 1	0.919	0.694	0.140	0.214
Measurement Point 2	0.971	0.471	0.339	0.192
Measurement Point 3	0.979	0.191	0.457	0.097
Measurement Point 4	0.967	0.089	0.468	0.037
Measurement Point 5	0.979	0.365	0.412	0.155

Table 4 Statistical summary of measured values, predicted values, and residuals for each measurement point.

Point	x (m)	$n=1$ meas	$n=1$ pred	$n=1$ resid	$n=2$ meas	$n=2$ pred	$n=2$ resid	$n=3$ meas	$n=3$ pred	$n=3$ resid	$n=4$ meas	$n=4$ pred	$n=4$ resid
1	11.110626	0.919000	0.908929	0.010071	0.694000	0.693167	0.000833	0.140000	0.145475	-0.005475	0.214000	0.213668	0.000332
2	12.610626	0.971000	0.961008	0.009992	0.471000	0.471599	-0.000599	0.339000	0.336742	0.002258	0.192000	0.188273	0.003727
3	14.110626	0.979000	0.990003	-0.011003	0.191000	0.204990	-0.013990	0.457000	0.456369	0.000631	0.097300	0.092669	0.004631
4	15.610626	0.979000	0.995217	-0.016217	0.089100	0.081198	0.007902	0.468000	0.478906	-0.010906	0.037100	0.037492	-0.000392
5	17.110626	0.985000	0.976524	0.008476	0.365000	0.359630	0.005370	0.412000	0.399559	0.012441	0.155000	0.153672	0.001328

Table 5 Statistical summary of mode shape fitting accuracy at each measurement point.

Mode	A_n	$n\pi/L_{\text{eff}}$	SSE	RMSE
$n=1$	0.996172	0.103337	0.000657	0.011464
$n=2$	0.928158	0.206753	0.000288	0.007590
$n=3$	0.483070	0.310130	0.000309	0.007864
$n=4$	0.215107	0.413507	0.000169	0.005818

3.4 Multi-case fitting analysis

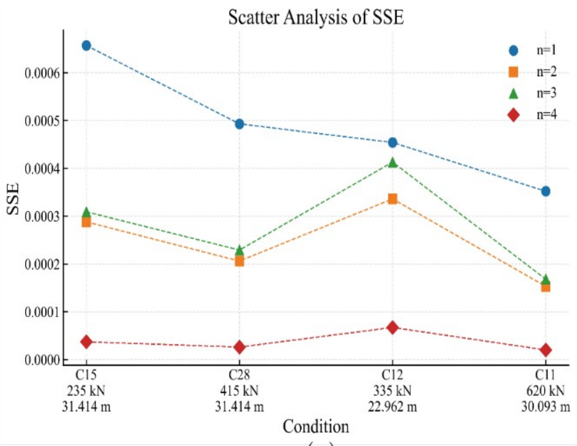

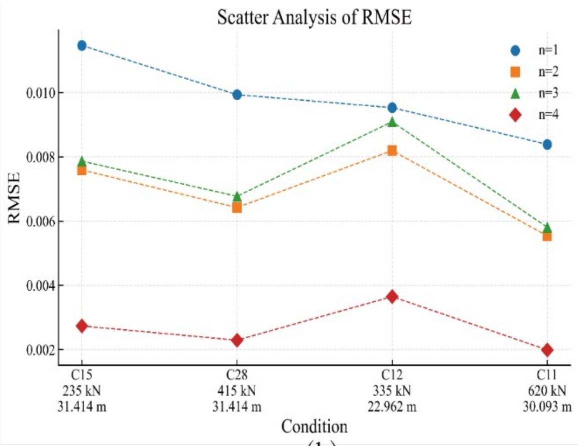

Statistical comparison of mode-shape fitting errors under different cable conditions: (a) SSE; (b) RMSE.

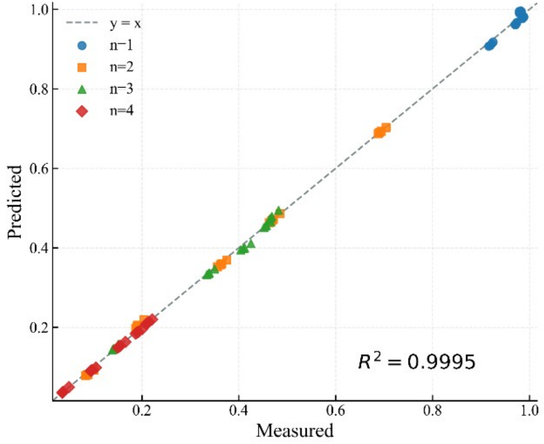

Comparison of measured and predicted mode-shape amplitudes.

Table 6 Identification results of effective vibration length and fitting errors under different cable conditions.

Cable ID	Cable tension (kN)	L (m)	L_{eff} (m)	Total SSE	Overall RMSE
C15	235	31.414	30.374	0.001291	0.008034
C28	415	31.414	30.434	0.000955	0.006909
C12	335	22.962	22.041	0.001269	0.007966
C11	620	30.093	29.277	0.000693	0.005887

- The first-order mode is most sensitive to sag effects.
- Use the 2nd–4th modes for effective vibration length identification.

3.5 Cable tension results

$$w(0,t)=0, \quad w(L,t)=0$$
$$w''(0,t)=0, \quad w''(L,t)=0$$

$$T=\mu\left(\frac{2Lf_n}{n}\right)^2 - EI\left(\frac{n\pi}{L}\right)^2 \quad (n=1,2,3...)$$

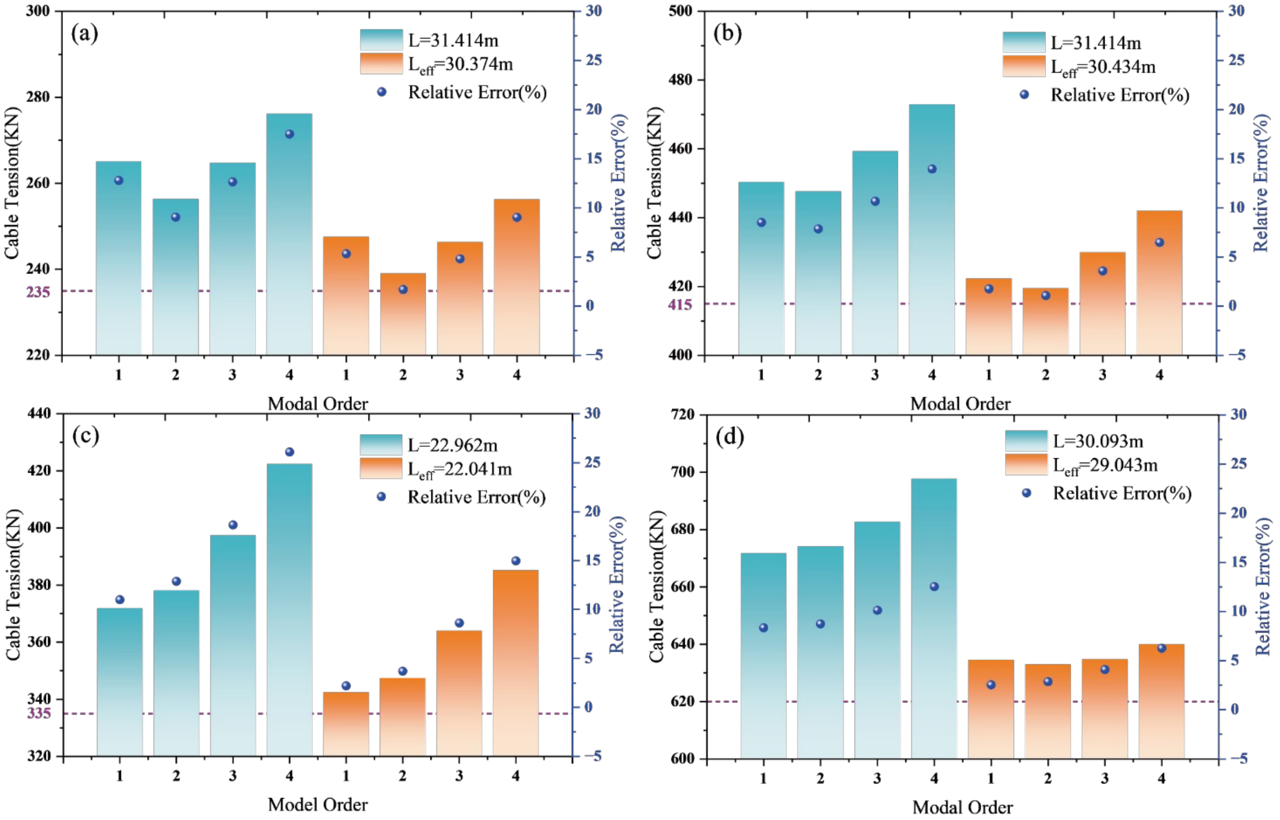

Comparison of cable tension calculation results using the actual length and effective vibration length.

3.5 Cable tension results

Table 7 Comparison of cable tension calculation results using actual length and effective vibration length.

(a) Cable #15

Cable #15	L=31.424 m				L_{eff}=30.374 m			
Modal Order	1	2	3	4	1	2	3	4
Frequency (Hz)	1.510	2.984	4.581	6.302	1.510	2.984	4.581	6.302
Tension (kN)	265.04	256.27	264.71	276.16	247.51	238.98	246.30	256.22
Error (%)	12.78	9.05	12.64	17.51	5.32	1.69	4.81	9.03

(b) Cable #28

Cable #28	L=31.424 m				L_{eff}=30.434 m			
Modal Order	1	2	3	4	1	2	3	4
Frequency (Hz)	1.967	3.933	6.002	8.167	1.967	3.933	6.002	8.167
Tension (kN)	450.31	447.61	459.30	472.90	422.28	419.43	429.87	441.88
Error (%)	8.51	7.86	10.67	13.95	1.75	1.07	3.58	6.48

(c) Cable #12

Cable #12	L=22.962 m				L_{eff}=22.041 m			
Modal Order	1	2	3	4	1	2	3	4
Frequency (Hz)	2.449	4.969	7.711	10.719	2.449	4.969	7.711	10.719
Tension (kN)	371.86	378.13	397.43	422.40	342.37	347.40	363.92	385.15
Error (%)	11.00	12.88	18.64	26.09	2.20	3.70	8.63	14.97

(d) Cable #11

Cable #11	L=30.093 m				L_{eff}=29.277 m			
Modal Order	1	2	3	4	1	2	3	4
Frequency (Hz)	2.508	5.035	7.625	10.322	2.508	5.035	7.625	10.322
Tension (kN)	671.71	674.12	682.71	697.69	634.50	632.94	634.66	639.88
Error (%)	8.34	8.73	10.11	12.53	2.53	2.85	4.08	6.26

Errors were reduced by 7.36%, 6.79%, 9.18%, and 5.88% compared with actual-length-based calculations

Main conclusions

(1) High-accuracy cable force estimation was achieved.

Using the effective vibration length and the second-order frequency, the relative errors of four cables were reduced to **1.69%, 1.07%, 3.70%, and 2.85%**, with error reductions of **7.36%, 6.79%, 9.18%, and 5.88%** compared with actual-length-based calculations.

(2) SSD-CEEMDAN effectively suppresses UAV drift.

The proposed drift separation method adaptively removes low-frequency UAV drift without preset cutoff frequencies, while preserving the dominant modal vibration components.

(3) Multi-order mode-shape consistency improves L_eff identification.

Joint fitting of multiple modes improves the stability and uniqueness of effective vibration length identification, providing reliable support for high-precision cable force inversion.

Future work

(1) Pre-applied cable markings.

Pre-applying strip markings during cable manufacturing can improve field efficiency and provide denser spatial constraints for mode-shape fitting.

(2) IMU/GNSS-assisted UAV drift correction.

Integrating IMU and GNSS data can help reconstruct UAV motion trajectories and further reduce drift-induced errors in low-frequency vibration identification.

(3) Extension to other structures.

Future work will validate and extend the proposed method to other structures, such as bridges, towers, and buildings.

Thank you ！